THE JOURNAL OF PHYSICAL CHEMISTRY B

ARTICLE

pubs.acs.org/JPCB

Phase Characterization and Study of Molecular Order of a Three-Ring Mesogen by ^{13}C NMR in Smectic C and Nematic Phases

S. Kalaivani and T. Narasimhaswamy

Polymer Laboratory, Central Leather Research Institute (Council of Scientific & Industrial Research, CSIR), Adyar, Chennai 600 020, India

Bibhuti B. Das,[†] Nitin P. Lobo,[†] and K.V. Ramanathan*[,‡]

[†]Department of Physics and [‡]NMR Research Center, Indian Institute of Science, Bangalore 560 012, India

Supporting Information

ABSTRACT:

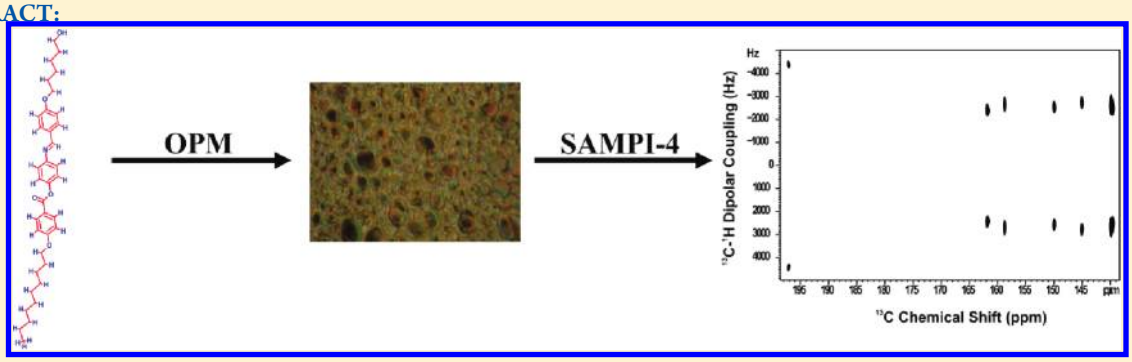

Molecules exhibiting a thermotropic liquid-crystalline property have acquired significant importance due to their sensitivity to external stimuli such as temperature, mechanical forces, and electric and magnetic fields. As a result, several novel mesogens have been synthesized by the introduction of various functional groups in the vicinity of the aromatic core as well as in the side chains and their properties have been studied. In the present study, we report three-ring mesogens with hydroxyl groups at one terminal. These mesogens were synthesized by a multistep route, and structural characterization was accomplished by spectral techniques. The mesophase properties were studied by hot-stage optical polarizing microscopy, differential scanning calorimetry, and small-angle X-ray scattering. An enantiotropic nematic phase was noticed for lower homologues, while an additional smectic C phase was found for higher homologues. Solid-state high-resolution natural abundance ^{13}C NMR studies of a typical mesogen in the solid phase and in the mesophases have been carried out. The ^{13}C NMR spectrum of the mesogen in the smectic C and nematic phases indicated spontaneous alignment of the molecule in the magnetic field. By utilizing the two-dimensional separated local field (SLF) NMR experiment known as SAMPI4, $^{13}C-^{1}H$ dipolar couplings have been obtained, which were utilized to determine the orientational order parameters of the mesogen.

INTRODUCTION

Thermotropic mesophases represent unique states of matter where partial order exists on a molecular and supramolecular level.[1−3] Molecules exhibiting mesophases are easily influenced by external stimuli and adopt a new configuration of minimum energy.[2] The calamitic mesogens are rod-like in nature and generally consist of a rigid core with linking units and terminal groups.[4] By a judicious choice of these structural components, a wide range of mesogens exhibiting both smectic and nematic phases have been synthesized.[5] However, in recent years, the molecular designing of mesogens has undergone a dramatic change. While the conventional approach to the design of the mesogen is based on parameters like geometrical anisotropy, linearity, and anisotropic polarizability,[6] the current view emphasizes molecular shape and topology, reduced symmetry, microphase segregation, self-assembly, and self-organization.[1−3,7−9] More recently, amphiphilic polyhydroxy compounds and carbohydrate derivatives have received special attention as they form both lyotropic and thermotropic mesophases. It is found that the morphologies of these thermotropic mesophases can be tailored by variation of the number and position of the −OH groups as well as the lipophilic chains.[10] As a consequence, the introduction of the hydroxyl group as a part of thermotropic mesogens and the study of such mesogens have gained importance.

Received: April 11, 2011
Revised: August 3, 2011
Published: August 30, 2011

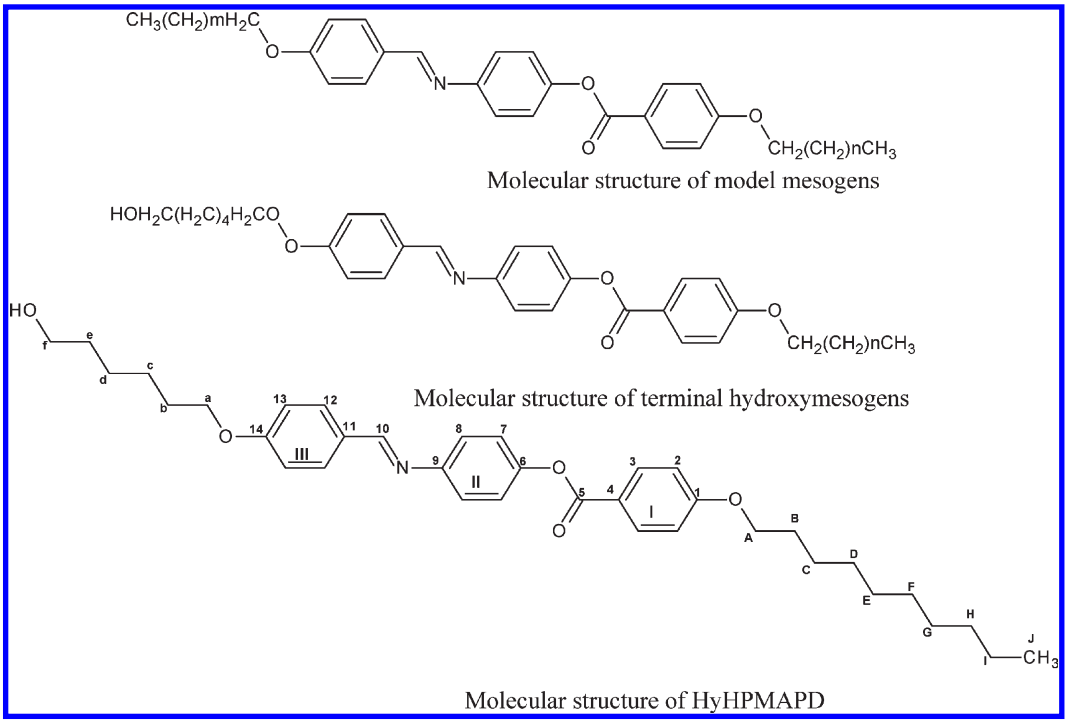

Figure 1. Molecular structure of mesogens.

The understanding of mesophase morphologies at the molecular level requires a thorough investigation of intermolecular interactions and their influence on the orientational order, which can be determined by many techniques.[11] Among them, solid-state NMR has acquired popularity and has become a standard technique in recent years since it is able to provide extensive information on local order and dynamics.[12−15] Deuterium NMR spectroscopy is a powerful technique for obtaining the molecular dynamics and order of mesogens.[16,17] However, it requires uniform/selective deuterium labeling of the sample. It has been shown in recent years that the natural abundance ^{13}C NMR technique is a useful alternative capable of providing extensive information about the mesophase.[18,19] The application of the two-dimensional separated local field (SLF) NMR technique provides $^{13}C-^{1}H$ dipolar couplings and, together with the ^{13}C chemical shifts, can be used to obtain the order parameters of various segments of the molecule, such as the rigid core and the terminal groups, and to study the molecular topology.[20,21]

In the present work, the mesogen core is designed to have three phenyl rings linked at the 1,4-position, connected via ester and azomethine groups. One of the terminal units has a hydroxy hexyloxy chain, while the other end has an alkoxy chain with an even number of carbons between 4 and 12. The commonly used linking units such as ester and azomethine are preferred as the ester is relatively stable and imparts a certain degree of polarizability while the azomethine contributes higher thermal stability and results in polymesomorphism.[22] Usually, three-ring-based mesogens possess a higher aspect ratio, in contrast to the two-ring homologues, and accordingly exhibit higher mesophase thermal stability,[23] while four- and five-ring-based cores result in higher melting and clearing temperatures, and their lower homologues often undergo decomposition.[22] Although the influence of phenolic OH on the mesophase characteristics of calamitics is known,[24,25] the effect of alcoholic OH as a terminal functionality has not been widely investigated. Here, we report structural characterization of mesogens with a three-ring core and a terminal hydroxyl by spectral techniques and phase characterization by hot-stage optical polarizing microscopy (HOPM), differential scanning calorimetry (DSC), and small-angle X-ray scattering (SAXS). One of the terminal hydroxyl mesogens has been studied using natural abundance ^{13}C NMR spectroscopy in the solid, smectic C, and nematic phases. In the mesophase, by employing the 2D SLF NMR technique, the $^{13}C-^{1}H$ dipolar couplings have been obtained to determine the orientational order at various temperatures. Owing to the presence of terminal hydroxyl, the mesogens may be classified as a reactive liquid crystal and can be suitably modified to get mesogenic monomers for side-chain liquid-crystalline polymers.[26]

EXPERIMENTAL SECTION

Three-ring mesogens with a hydroxy hexyloxy chain at one end and an alkoxy chain (even number of carbons 4−12) at the other have been synthesized (Figure 1). The model mesogens with terminal methyl have also been obtained for comparing the mesophase characteristics with terminal hydroxyl series. The synthetic details and spectral data are furnished in the Supporting Information.

Solid-State NMR Studies. Solid-state NMR experiments were performed on a Bruker AVIII 500 WB NMR spectrometer. The proton and carbon resonance frequencies were 500.17 and 125.79 MHz, respectively, corresponding to a magnetic field of 11.75 T. ^{13}C CP/MAS spectra of one of the mesogens was recorded at room temperature in the crystalline phase using a 4 mm MAS probe. A sample spinning speed of 5 kHz was used, and the TOSS[27] pulse sequence was employed to avoid spinning sidebands. Typically, 512 scans were used with a relaxation delay of 3 s to acquire the time domain signal. Exponential apodization was used with a line broadening constant of 12 Hz before Fourier transformation to obtain the frequency domain spectrum.

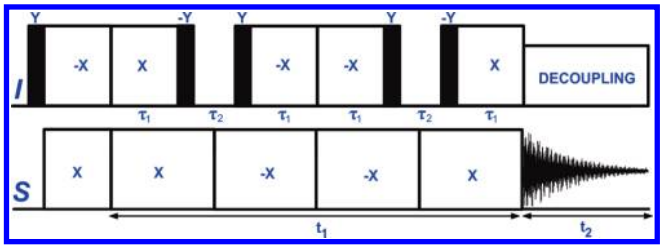

Figure 2. SAMPI4 pulse sequence used for obtaining the 2D-SLF spectrum in the mesophase.

The spectra in the liquid-crystalline phase of the same sample were obtained in the range between 120 and 180 °C using a double-resonance probe equipped with a 5 mm solenoid coil for static samples. In this temperature range, the sample exhibited smectic C and nematic phases. The sample was observed to align spontaneously in the magnetic field and provide sharp well-resolved lines. Because the anisotropic interactions are only partially averaged, ^{13}C spectra could be recorded by employing Hartmann−Hahn cross-polarization. During acquisition of the signal, heteronuclear dipolar decoupling was employed using the SPINAL-64 sequence.[28] Typically, 512 scans with a delay of 15 s between scans to avoid sample heating due to rf were used to obtain a spectrum with a good S/N ratio.

Partially averaged $^{13}C-^{1}H$ dipolar couplings of the sample were obtained using the SLF two-dimensional NMR spectroscopy. For this purpose, the SAMPI4 pulse sequence[29] (Figure 2) was applied on the oriented sample under static conditions. This pulse sequence is similar to the PISEMA[30] pulse sequence, and during the t_1 period, magnetization exchange between protons and carbons takes place under Hartmann−Hahn match. However, it differs from PISEMA in that for homonuclear proton dipolar decoupling, the Lee−Goldburg (LG) sequence used in PISEMA is replaced with a modified magic sandwich pulse sequence.[31] The purpose of including homonuclear decoupling during t_1 is to minimize magnetization decay through proton spin diffusion, thereby achieving line narrowing in the F_1 dimension. During the t_2 period, the carbon chemical shift spectrum with proton decoupling is acquired. A two-dimensional Fourier transform yields a 2D spectrum with carbon chemical shifts along the F_2 axis. The cross-peaks observed along the F_1 dimension provide the proton−carbon dipolar couplings. In order to maximize the polarization transfer and get higher intensities in the 2D plots, polarization inversion is used,[32] in which carbons are initially polarized using a CP contact time of 2 ms. The spectra were recorded by using 62.5 kHz of rf for both the proton and carbon channels during the t_1 period. During the t_2 period, a broad-band heteronuclear decoupling pulse scheme SPINAL64[28] with 30 kHz of rf was used. The homonuclear dipolar decoupling sequence used during the t_1 period is based on the idea that the homonuclear dipolar coupling in the rotating frame under spin-lock is half of its value in the laboratory frame and is of opposite sign.[33] Therefore, evolution of magnetization alternately under rotating and laboratory frames produces echoes, indicating removal of the interaction over one cycle.[34] The $\pi/2$ pulses that sandwich the τ_2 period in Figure 2 ensure cycling of the magnetization through the rotating frame during the two τ_1 periods and the laboratory frame during the τ_2 period. The τ_1 and τ_2 ideally should be the same. However, to take care of magnetization evolution during the nonideal $\pi/2$ pulses, τ_1 and τ_2 are adjusted to be equal to $7\pi/4\omega_1$ and $6\pi/4\omega_1$, where ω_1 is the rf field strength.[29] In the present

Scheme 1. Multistep Synthetic Route for Model and Target Mesogens[a]

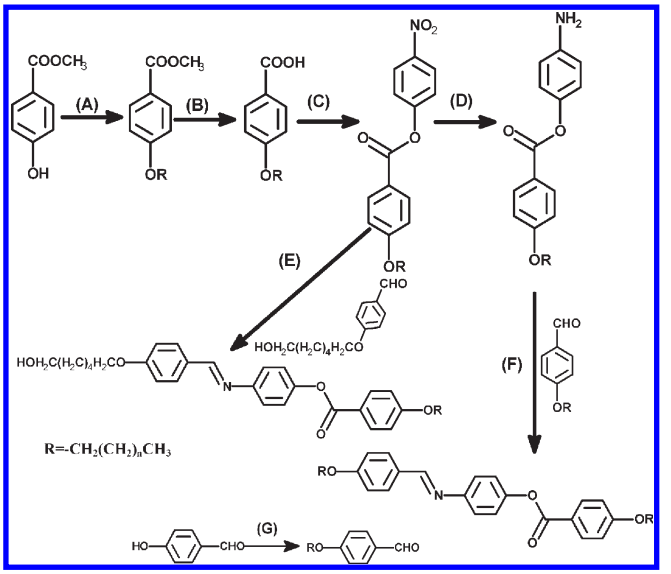

[a] (A) DMF/K_2CO_3/90 °C/RBr (C4−C12 even only); (B) EtOH/KOH; (C) 4-nitrophenol/DCC/DMAP; (D) Pd/C, THF/EtOH; (E,F) EtOH/AcOH, reflux; (G) RBr or 6-chloro hexanol/ DMF/K_2CO_3/90 °C.

experiment, values of τ_1 and τ_2 were respectively 14 and 12 μs. The pulse sequence uses a supercycle with two dwell periods with rf phases in mirror symmetry, which suppresses odd-order perturbative terms of the dipolar Hamiltonian. In addition, the use of the supercycle makes the measurement of dipolar coupling less susceptible to proton chemical shift and offset compared to PISEMA. Theoretical calculations have been used to derive the scale factor of the sequence, which is nearly equal to unity.[29] In our case, we recorded the 1D fully proton coupled ^{13}C spectrum of chloroform oriented in the liquid crystal *N*-(4-ethoxybenzylidine)-4-*n*-butylaniline (EBBA) and also the 2D-SAMPI4 spectrum of the same sample. The dipolar doublet splitting obtained in the former experiment was used to estimate the scaling factor for the latter. The frequency scale in the F_1 dimension during data processing has been adjusted to take care of the scale factor, so that the actual dipolar frequencies can be read out from the 2D plots and 1D cross section. Typically, 16 transients were used for each t_1 period with a recycle delay of 15 s between scans and 128 t_1 increments were employed. A shifted sine bell window function was applied to the time domain data, and the spectra were processed in the phase-sensitive mode.

RESULTS AND DISCUSSION

The synthesis of mesogens is accomplished as depicted in Scheme 1. The key intermediate 4-alkoxybenzoyloxy aniline is reacted with 4-[(6-hydroxyhexyl)oxy]benzaldehyde to get target mesogens and are named as the 6 series. In order to compare and understand the influence of the hydroxyl group on the mesophase characteristics, compounds with a terminal methyl group at both the ends have also been synthesized, which serve as model compounds (Figure 1). All of the synthesized mesogens have been characterized by FT-IR and ^{1}H and ^{13}C NMR spectroscopy. The spectral data for a representative mesogen is furnished in the

Supporting Information. Figure 1 shows the molecular structure of the mesogens.

The hot-stage optical polarizing microscopy studies of the mesogens showed enantiotropic mesophases. Table 1 lists the melting and the clearing temperatures along the with transition enthalpy (ΔH) values of all of the synthesized mesogens. Among the three model mesogens, lower homologue HPMAPB showed the enantiotropic nematic phase, while the higher homologues HPMAPD and HPMAPDd exhibited both smectic C and nematic phases, respectively (Table 1). For those with the hydroxy terminal, the lower homologues, that is, HyHPMAPB and HyHPMAPH showed enantiotropic nematic phases similar to the corresponding model compounds, whereas the higher homologues HyHPMAPO, HyHPMAPD, and HyHPMAPDd exhibited both smectic C and nematic phases. For instance, the OPM textures of the HyHPMAPD (Figure 3) while cooling the isotropic phase shows nematic droplets that coalesce to give a marble texture (Figure 3A). Upon further cooling, the mesogen changes to the smectic C phase, as indicated by the transition bars (Figure 3B), and exhibits smectic schlieren texture. The microscopic data is also confirmed by transition enthalpy (ΔH) values determined from differential scanning calorimetry (Table 1). The HOPM and DSC studies thus clearly indicate the appearance of the smectic C phase for higher homologues. It is also observed that the temperature range of the smectic C phase for the terminal hydroxyl mesogens is reduced in comparison to that of the corresponding model compounds. This may be attributed to the terminal interactions involving the hydroxyl group through hydrogen bonding. While it may be concluded that the overall molecular anisotropic polarizability is high in these systems, as suggested by the thermal stability values, a marginal increase in the melting point also indicates that the terminal attractions do play a role in influencing the mesophase characteristics.

SAXS Studies. The mesophase sequence for HyHPMAPD, as mentioned above, was first observed by hot-stage polarizing microscopy and was later confirmed by DSC. In order to further establish the layer ordering of the mesogen, SAXS studies were carried out at various temperatures. The measurements were carried out using a Bruker Nanostar instrument equipped with a rotating anode source and a three-pinhole collimation system with pinhole diameters for high flux (μm), 750, 400, and 1000. The wavelength of the X-rays was 1.54 Å (Cu K_α radiation) operated at 45 kV/110 mA. SAXS data were recorded in the q range of 0.05−0.72 (1/Å). A distance of 26 cm was maintained between the sample and detector. For data collection, the sample was sandwiched between two pieces of scotch tape of known thickness, and the backgrounds were subtracted from that of blank scotch tape. The sample exposure time was 900 s, and the ramp rate was 6 °C/min. Once the target temperature was reached, a 300 s delay was used before starting the experiment. The results of the studies are depicted in Figure 4.

The SAXS trace of HyHPMAPD at 118 °C shows two sharp peaks at q = 0.1166 and 0.234, which are assigned to first- and second-order Bragg reflections, the latter being of low intensity. The corresponding layer spacings ($d = 2\pi/q$; $d = 4\pi/q$) of these reflections are 53.88 and 53.70 Å. These reflections clearly suggest a layer ordering typical of smectic phases.[35] Further, with the increase in temperature, an increase in layer spacing is observed. Thus, the measurements at 127 and 136 °C also show two sharp peaks but with increased layer spacings of 54.16 and 55.21 Å, respectively, obtained from first-order reflections. This suggests that the phase under investigation is the smectic C as the tilt angle decreases with temperature. In the nematic phase at

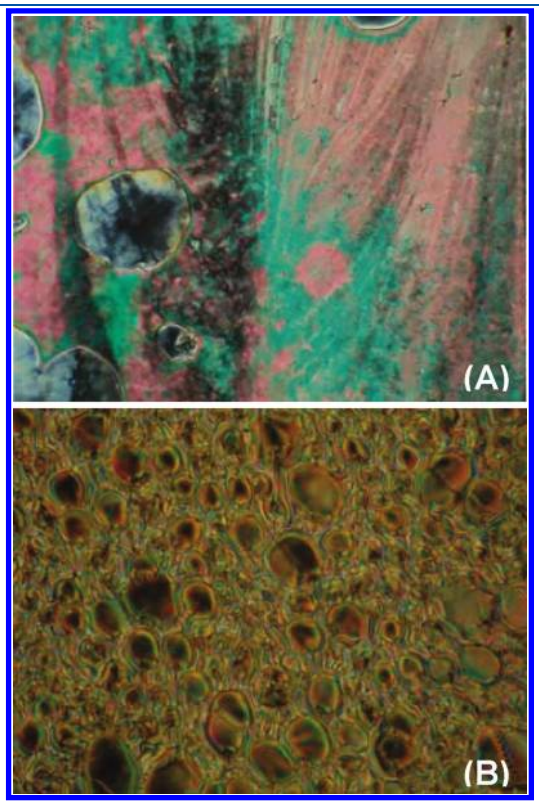

Figure 3. Optical polarizing micrographs of HyHPMAPD. (A) At 201 °C in the cooling cycle showing the marble texture of the nematic phase. (B) Characteristic transition bars near transition from the nematic to smetcic C phase at 137 °C.

Table 1. OPM and DSC Phase Transition Data of the C6 Series[a]

S. No	code	m	n	T_{C-Sc} °C	T_{C-N} °C	T_{Sc-N} °C	T_{N-I} °C	ΔT_{Sc}	ΔT_N
1	HPMAPB	4	2		113.3 (7.83)		242.4 (0.44)		129.1
2	HPMAPD	4	8	104.8 (7.64)		142.6 (0.39)	207.3 (0.37)	37.8	64.7
3	HPMAPDd	4	10	98.8 (6.70)		147.2 (0.47)	197.6 (0.41)	48.4	50.4
4	HyHPMAPB	4	2		125.6 (5.09)		238.9 (0.46)		113.3
5	HyHPMAPH	4	4		127.2 (6.79)		223.5 (0.60)		96.3
6	HyHPMAPO	4	6	110.2 (9.39)		120.5 (1.10)	213.7 (0.73)	10.3	93.2
7	HyHPMAPD	4	8	108.9 (7.23)		137.7 (0.99)	202.7 (0.47)	28.8	65.0
8	HyHPMAPDd	4	10	109.5 (8.54)		149.7 (1.18)	194.7 (0.42)	40.2	45.0

[a] Values in the parentheses indicate ΔH in kcal/mol.

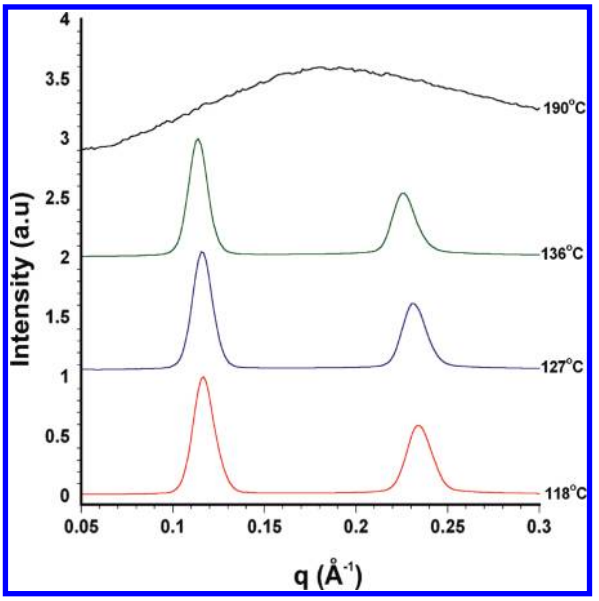

Figure 4. Variable-temperature SAXS traces of HyHPMAPD in smectic C and nematic phases.

190 °C, however, the sharp peaks that are noticed at lower temperatures are replaced by a broad hump, indicating liquid-like ordering. These features unambiguously confirm the existence of smectic C and nematic phases in HyHPMAPD.

^{13}C NMR Studies of HyHPMAPD. *Spectral Assignment in Solution.* For the study of molecular dynamics and orientational order in the mesophase by NMR, the first step is the assignment of the spectrum to the molecular structure of the mesogen in solution. The proton-decoupled ^{13}C NMR spectrum of HyHPMAPD in solution is shown in Figure 5A. The molecule consists of three phenyl rings joined by two linking units in the core and is flanked by terminal hydroxyl and decyloxy chains (Figure 1). The individual assignment of the chemical shifts of all of the carbons is carried out by comparing structurally similar compounds and also using the iterated spectrum generated by the ACD Chemsketch (version 3.0) software. The assigned chemical shift values along with the carbon numbers are listed in Table 2. The solution NMR spectrum showed 14 well-resolved lines in the region of 113−166 ppm and accounted for all 20 carbons of the core unit. The highly intense signals in the region of 113−133 ppm arise from the protonated carbons of the phenyl rings. The chemical shift equivalence of the carbons at the ortho and the meta positions indicate rapid π-flips of the phenyl rings about their C_2 axes. The azomethine carbon showed a sharp line of higher intensity at 159.8 ppm due to its attached proton giving rise to a shorter relaxation time in comparison to the quaternary carbons, which showed well-resolved lines of lower intensity in this region. Thus, among the 14 lines, 7 have been assigned to the methine carbons and the remaining to the quaternary carbons. In the aliphatic region (13−69 ppm), 13 lines are seen with varying intensity accounting for 16 carbons arising from the terminal hydroxy hexyloxy and decyloxy chains. Table 2 shows the assignment of these lines to various methylenes and a methyl carbon. Among them, three lines are seen at 63−69 ppm with equal intensity. The larger chemical shift values of these lines, in contrast to other signals in the region, indicate that they are from $-OCH_2$ carbons. Because the mesogen consists of a hydroxyl hexyloxy chain at one end and a decyloxy chain at the other, two lines from the $-OCH_2$ groups and one line corresponding to the $-CH_2OH$ carbon are expected. Of them, the chemical shift values of the two $-OCH_2$ carbons are very similar, and the corresponding signals appear at a higher frequency due to their proximity to the phenyl rings. The line appearing at the lower frequency may be assigned to the $-CH_2OH$ carbon. In the region of 22−33 ppm, nine lines are observed, which are from the decyloxy chain and central methylenes of the hydroxyl hexyloxy chain. The characteristic methyl carbon of the decyloxy chain is noticed at 14.13 ppm.

^{13}C CP/MAS NMR Study of Crystalline HyHPMAPD. To study the mesogen in its solid phase, the ^{13}C CP/MAS spectrum of the compound is obtained at room temperature. The sample is spun at 5 kHz, and to eliminate the spinning sidebands, the spectrum is obtained using the TOSS pulse sequence.[27] The spectrum (Figure 5B) shows 24 peaks in the region of 110−170 ppm, in contrast to 14 lines in the solution spectrum. The increase in the number of lines compared to the solution state spectrum indicates the presence of either more than one molecule in the unit cell or molecules with different conformations. A closer examination of the chemical shift values shows that 6 out of the 10 additional peaks observed fall in the region of 110−134 ppm and are attributable to the phenyl ring methine carbons. The remaining four signals occurring in the region of 142−158 ppm may be assigned to quaternary carbons. For the terminal chains, additional peaks are also seen in the region of 60−70 ppm, while the methylene region (20−35 ppm) showed a set of broad peaks, in contrast to the solution spectrum, due to overlapping of methylene carbon chemical shifts. In an earlier work, a structurally similar nematogen also showed more peaks in the solid state at room temperature that however disappeared when the temperature of the sample was raised.[36]

^{13}C NMR Spectrum of HyHPMAPD in the Mesophase. Figure 5C and D shows the ^{13}C NMR spectrum of a static sample of the mesogen in its smectic C phase at 120 °C and in the nematic phase at 160 °C. In contrast to CP/MAS and solution spectra, the peaks in the mesophase are observed to be well-dispersed. The other notable feature of the spectra in the mesophase is the reduction in the number of peaks as compared to the spectrum in the solid state; the number is now akin to that in the spectrum in the solution phase. There is also a dramatic change in the chemical shift values, which cover a much larger range. The peaks that are seen in the solution and in the solid state in the range of 113−166 ppm now appear at a higher frequency in the region of 140−250 ppm. On the other hand, the signals that are seen in the range of 13−69 ppm in the solution and in the solid state are slightly shifted to the lower frequency and appear in the region of 8−60 ppm. Observation of the sharp peaks and the spread in the chemical shift values clearly indicate that the sample in the smectic C and the nematic phases are oriented in the magnetic field. The changes observed in the chemical shift values of the mesogen upon going to the mesophase suggest that the molecules are aligned parallel to the field. These are confirmed subsequently from the order parameters obtained from dipolar couplings. It is seen in the spectrum that the line widths in the smectic C phase are relatively large compared to those obtained in the nematic phase.

The assignment of the chemical shift values of the aligned mesogens to individual carbons is difficult. This is due to the lack of data on the chemical shielding tensors of different carbons belonging to different groups involved in the construction of the mesogen and also due to the possibility of a difference in the

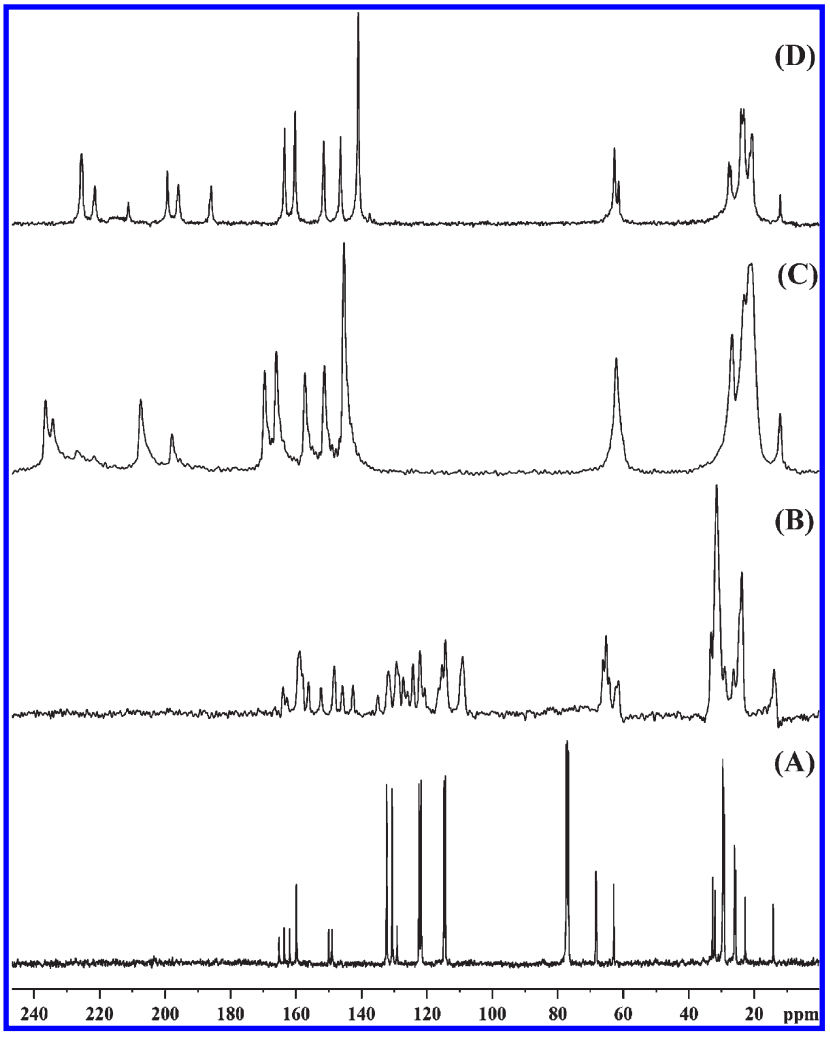

Figure 5. (A) Proton-decoupled ^{13}C NMR spectrum of HyHPMAPD in solution at 25 °C. (B) ^{13}C CP/TOSS NMR spectrum of HyHPMAPD with 5 kHz spinning speed at 25 °C in the solid phase. (C) ^{13}C spectrum of the static oriented sample of HyHPMAPD at 120 °C in the smectic C phase. (D)^{13}C spectrum of the static oriented sample of HyHPMAPD at 160 °C in the nematic phase.

ordering along the length of the molecule. Gross assignments may be made from the peak positions and intensities, while finer assignments can be done by comparison of the spectral pattern with those of structurally similar compounds and model mesogens for which the assignments are already known. The procedure adopted for assigning the spectrum in the smectic C phase is described below, and assignment in the nematic phase follows as an extension of the same logic. In the smectic C phase, the ring 1 chemical shifts have been assigned by comparing with the static ^{13}C NMR spectrum of structurally similar mesogens.[19,37]

As a result of the π flips that phenyl rings undergo about the para-axis, a single line is observed for the pair of methine carbons in the ortho and meta positions. Consequently, 6 peaks may be expected, corresponding to the 12 methine carbons in the three phenyl rings. However, the spectrum shows only five peaks in the region of 140−180 ppm. In view of the ortho carbons in ring 3 (carbons 13 and 13′) having a chemical environment similar to carbons 2 and 2′ in ring 1, the overlap of corresponding signals is possible. In solution too, these carbons show two closely spaced lines at 114.76 and 114.37 ppm. In the spectrum in the mesophase, the peak that appears at 145.3 ppm is more intense and can account for four carbons. Hence, this peak is assigned to carbons at positions 2/2′ and 13/13′. The azomethine carbon has been identified by considering the intensity and chemical shift value and assigned to the peak at 207.4 ppm, which is further supported by the SLF-2D data presented in the next section. On the basis of the intensity pattern and by comparison with the chemical shifts of other structurally similar mesogens, the other aromatic methine carbons of the static spectrum have also been assigned, and the chemical shift values are listed in Table 2. In contrast to the spectrum in solution, the ^{13}C NMR spectrum in the mesophase shows only three signals for quaternary carbons, whereas the core unit of the mesogens consists of seven quaternary carbons. However, in the 2D spectrum, four peaks can be identified for the quaternary carbons. The signal appearing at 236.4 ppm has a higher intensity compared to other peaks in the region and may be attributed to overlapped lines of structurally similar carbons like C1, C6, and C14. The ester carbonyl carbon C5 is assigned a chemical shift of 226.6 ppm. Of the other three quaternary carbons, C4 is assigned to the peak at 197.7 ppm, while C9 and C11 are assigned to 234.3 and 207.4 ppm, respectively (Table 2). In the case of aliphatic chains, by close observation of the region of 50−60 ppm and also with the help of the 2D-SLF spectrum, two

Table 2. ^{13}C Chemical Shifts (ppm) of HyHPMAPD in Solution, Solid, and Smectic C and Nematic Phases

carbon code	solution (ppm) 25 °C	solid CP-MAS (TOSS)- (ppm) 25 °C	smectic C phase static (ppm) 120 °C	AIS (ppm) ($\delta_{lc} - \delta_{soln.}$)	nematic phase static (ppm) 160 °C	AIS (ppm) ($\delta_{lc} - \delta_{soln.}$)
1	163.6	163.9	236.4	72.8	222.2	58.6
2	114.3	114.3	145.3	31.0	139.7	25.4
3	132.3	131.8	169.5	37.2	161.6	29.3
4	121.7	120.6	197.7	76.0	182.7	61.0
5	165.1	163.9	226.6	61.5	208.6	43.5
6	148.9	148.2	236.4	87.5	222.2	73.3
7	121.7	122.0	151.3	29.6	144.9	23.2
8	122.3	122.0	157.1	34.8	139.8	17.5
9	149.9	152.3	234.3	84.4	217.7	67.8
10	159.8	158.8	207.4	47.6	197.1	37.3
11	129.0	128.5	207.4	78.4	192.8	63.8
12	130.5	129.2	165.8	35.3	158.6	28.1
13	114.7	115.3	145.3	30.6	139.7	25.0
14	161.9	162.7	236.4	74.5	222.2	60.3
A	68.3	66.1	62.1	−6.2	62.9	−5.4
a	68.1	65.1	62.1	−6.0	62.9	−5.2
f	62.8	62.3	61.5	−1.3	61.2	−1.6
e	32.7	33.1	26.8	−5.9	28.0	−4.7
B	31.9	31.5	26.8	−5.1	27.4	−4.5
G, H	29.5	31.5	23.0	−6.5	24.3	−5.2
E, F	29.3	31.5	23.0	−6.3	24.3	−5.0
b, D	29.1	31.5	23.0	−6.1	24.3	−4.8
c	26.0	26.3	21.5	−4.5	23.4	−2.6
d	25.9	24.5	21.5	−4.4	23.4	−2.5
C	25.5	23.8	20.6	−4.9	21.0	−4.5
I	22.7	23.8	20.6	−2.1	21.0	−1.7
J	14.1	14.0	12.1	−2.0	12.0	−2.1

peaks can be identified. Of them, the two $-OCH_2$ are assigned to 62.1 ppm, and the terminal $-CH_2OH$ is given an assignment of 61.5 ppm. All other methylene carbons appear in the region of 16.9 to 24 ppm as broad peaks due to overlap of signals from carbons with nearly the same chemical shift. The narrow chemical shift span for these carbons does not favor resolution of the peaks corresponding to the different carbon sites. The signal due to the methyl carbon of the decyloxy chain appears at 9.4 ppm.

The spectrum in the nematic phase (160 °C) (Figure 5D) shows similar trends with better resolution. For instance, in the smectic C phase, the quaternary carbon (C11) and the azomethine carbon (C10) appear as a single line due to overlap, but in the nematic phase, they appear as separate lines. Similarly, in the smectic C phase, in the aliphatic region, the signals due to $-OCH_2$ and CH_2OH carbons are overlapped. In the nematic phase, they are clearly separated into two lines. This improvement in resolution in the nematic phase results from smaller line width due to faster dynamics of the molecules and low molecular order compared to that of the smectic C phase.

The alignment-induced chemical shift (AIS) for all of the carbons has been obtained as the difference between the chemical shifts in the oriented phase and the isotropic phase ($\delta_{lc} - \delta_{solution}$) and are listed in Table 2, while Table 3 shows the chemical shifts of carbons of the core unit of the mesogen in both phases at different temperatures. As seen in Table 2, unlike the aliphatic carbons, the aromatic, the carbonyl, and the azomethine carbons (core unit carbons) have large AIS values due to the large span of their chemical shift tensors. Also, the quaternary carbons show a larger shift to the higher frequency than methine carbons. For instance, for the aromatic methine carbons C7 and C8 in the central phenyl ring, the AIS values are respectively 29.6 and 34.8 ppm, while the quaternary carbons C6 and C9 of the same ring have values of 87.5 and 84.4 ppm, respectively. These results are in conformity with behavior expected for mesogens that are aligned parallel to the field.[38]

2D-SLF. The SAMPI4 pulse sequence shown in Figure 2 has been used to obtain a two-dimensional SLF NMR spectrum of the aligned mesogens both in the smectic C and in the nematic phases. The experiment provides ^{13}C chemical shifts along the F_2 axis and $^1H-^{13}C$ dipolar couplings along the F_1 axis. Earlier use of SAMPI4 on a liquid-crystalline system is made on 4-*n*-pentyl-4′-cyanobiphenyl (5CB) to demonstrate its applicability and performance.[39] In this work, the use of SAMPI4 is presented for the first time for a novel mesogen. Figure 6 shows a typical 2D plot of the mesogen HyHPMAPD in its smectic C phase at 120 °C, and Figure 7 shows expanded plots of the aromatic methine signals of the 2D spectra in the smectic C (120 °C) as well as in the nematic (160 °C) phases. For the sake of clarity, the spectrum obtained in the smectic C phase at 120 °C (Figures 6 and 7A) is discussed in detail, while the data obtained at other temperatures in the smectic and nematic phases are listed in Table 3. In Figures 6 and 7, well-resolved cross-peaks along the F_1 axis can be seen for several carbons both for the core unit and for the terminal chains, with line widths in the F_1 dimension in

some cases being as low as 200 Hz. Interestingly, the line widths are reduced even further to 100 Hz by the use of maximum entropy reconstruction methods,[40] the details of which will be presented elsewhere. The additional resolution available in the 2D spectrum is used for confirmation of assignment of several carbons.

The core unit of HyHPMAPD consists of seven chemically inequivalent methine carbons. Among them, six carbons belong to the three phenyl rings, and the remaining one to the azomethine group. However, in the 2D spectrum (Figure 7), only six dipolar contours with a large separation along the dipolar dimension that could correspond to the aromatic methine carbons are observed. As in the case of the 1D spectrum, a close examination reveals that the contours at 145.3 ppm (Figure 7A) are more intense than others and also show a slightly larger spread in both dimensions. As discussed in the earlier section, these contours are attributed to the two methine carbons C2 and C13 belonging to the rings 1 and 3, respectively. The superposition of the contours of both of these carbons indicates that not only the chemical shifts but also the dipolar coupling values are nearly the same for both carbons. The other phenyl ring methine carbon contours are seen at 151.3, 157.1, 165.8, and 169.5 ppm, while the characteristic contours corresponding to the azomethine linking unit appears at 207.4 ppm. The 2D spectral pattern is thus consistent with the molecular structure. The frequencies of the contours along the dipolar dimension correspond to the dipolar oscillation frequencies (f_D) and are listed in Table 3. The dipolar oscillation frequency corresponds directly to the dipolar coupling only for an isolated C−H pair.[41] For more than two protons coupled to a carbon, the dipolar coupling information needs to be extracted from the oscillation frequency (vide infra). In Table 3 and Figure 7A, it is seen that the dipolar frequencies are not the same for all carbons in the core unit. Earlier studies of two ring nematogens show that typical dipolar oscillation frequencies for phenyl rings are about 2.00 kHz.[18] However, in the present case, these values are found to be around 3.00 kHz. Also the azomethine dipolar frequency of 5.55 kHz is significantly higher than the value of 3.5 kHz observed for mesogens like MBBA and EBBA. These observations indicate overall a high molecular order for HyHPMAPD in the smectic phase.

The 2D spectrum of the mesogen in the aliphatic region (9−70 ppm) also shows well-resolved signals. The high resolution observed in the 2D spectrum, compared to the 1D spectrum, arises out of the difference in the dipolar couplings of carbons whose signals are overlapped in the 1D spectrum due to nearly identical chemical shift values. For instance, the $-OCH_2$ and $-CH_2OH$ carbons whose peaks overlap and are just discernible

Table 3. Chemical Shifts (in ppm) and Dipolar Oscillation Frequencies (in kHz) of Carbons in the Aromatic Core Unit of HyHPMAPD at Different Temperature in the Mesophase

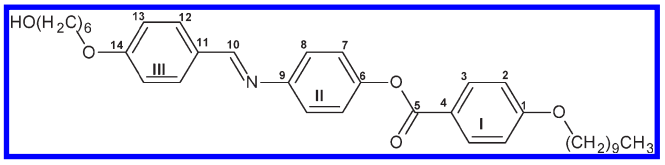

	120 °C		130 °C		140 °C		160 °C		180 °C	
C. No	ppm	kHz	ppm	kHz	ppm	kHz	ppm	kHz	ppm	kHz
1	236.4	1.84	235.2	1.83	228.4	1.57	222.2	1.46	212.2	1.21
2	145.3	3.24	144.7	3.18	142.1	2.87	139.7	2.60	135.3	2.15
3	169.5	3.02	168.7	2.98	165.0	2.69	161.6	2.41	156.3	1.98
4	197.7	1.71	196.5	1.74	188.8	1.56	182.7	1.44	172.3	1.13
5	226.6		226.1		213.6		208.6		201.4	
6	236.4	1.84	235.2	1.83	228.4	1.74	222.2	1.46	212.2	1.21
7	151.3	3.46	150.5	3.37	147.6	3.04	144.9	2.75	140.7	2.24
8	157.1	3.21	156.4	3.13	152.9	2.82	149.8	2.53	145.0	2.18
9	234.3	1.86	233.4	1.78	224.7	1.74	217.7	1.54	207.2	1.23
10	207.4	5.55	206.4	5.53	201.2	4.88	197.1	4.44	190.3	3.68
11	207.4	2.12	206.4	1.98	198.8	1.82	192.8	1.75	182.2	1.40
12	165.8	3.34	165.2	3.30	161.6	2.97	158.6	2.68	153.7	2.21
13	145.3	3.24	144.7	3.18	142.1	2.87	139.7	2.60	135.3	2.15
14	236.4	1.84	235.2	1.83	228.4	1.57	222.2	1.46	212.2	1.21

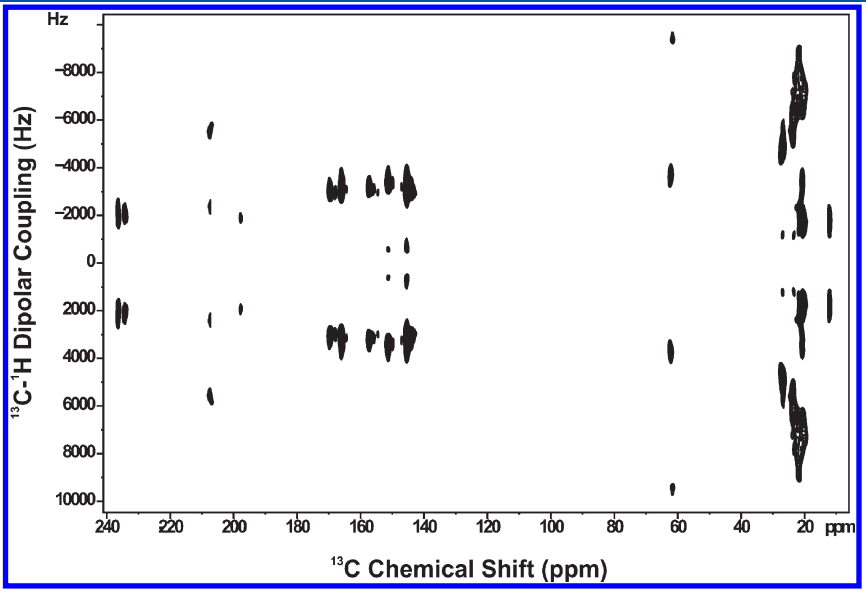

Figure 6. $^{13}C-^{1}H$ 2D-SLF spectrum of HyHPMAPD at 120 °C in the smectic C phase.

dx.doi.org/10.1021/jp203388v |J. Phys. Chem. B 2011, 115, 11554–11565

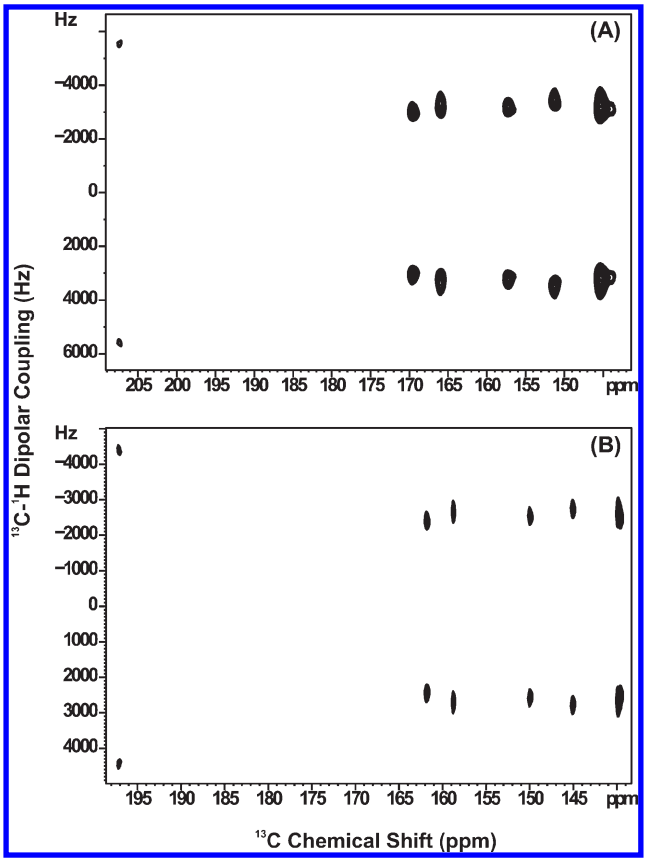

Figure 7. An expanded plot of the 2D-SLF spectrum of HyHPMAPD corresponding to the aromatic core; (A) smectic C phase (120 °C); (B) nematic phase (160 °C).

as two lines in the 1D spectrum are now separated into two sets of contours with dipolar oscillation frequencies of 9.4 and 3.71 kHz, respectively, for the $-OCH_2$ and $-CH_2OH$ carbons. This difference in the dipolar frequencies arises due to their locations in the mesogenic molecule. The $-OCH_2$'s are positioned closer to phenyl rings of the core unit, while the $-CH_2OH$ is at one terminal of the mesogens where the mobility is high. The dipolar couplings thus provide a valuable indicator of the local dynamics and the position of the atoms in the molecule. For the large number of $-CH_2$ carbons, the 1D spectrum shows one broad signal with few shoulders, whereas several contours are clearly distinguished in the range of 16.9−24 ppm in the 2D spectrum. The characteristic terminal methyl shows a contour at 9.9 ppm with a dipolar frequency of 1.91 kHz. No attempt is made here to further identify the chain carbons in view of the complex dynamics; subsequent discussion being confined to the aromatic core. From the experimentally measured $^{13}C-^{1}H$ dipolar frequencies, the orientational order parameters of the aromatic core of the liquid-crystal molecule have been obtained, which are presented in the next section.

Orientational Order Parameters. The smectic C phase exhibits biaxial ordering. However, for an aligned sample, the phase biaxiality may not be detected, and hence, only the molecular order parameters may be obtained.[42] The measured dipolar couplings can be used for estimating the local order parameters of the liquid-crystal fragments. The phenyl rings require two order parameters, namely, S'_{zz} and $S'_{xx} - S'_{yy}$, and the carbon−proton dipolar coupling in terms of these parameters is given by[12,20]

$$D_{C-H} = K\left\{\frac{1}{2}(3\cos^2\theta_z - 1)S'_{zz} + \frac{1}{2}(\cos^2\theta_x - \cos^2\theta_y)(S'_{xx} - S'_{yy})\right\} \quad (1)$$

where $K = -h\gamma_C\gamma_H/4\pi^2 r^3_{CH}$, with γ_C and γ_H being the gyromagnetic ratios of carbon and hydrogen nuclei, respectively, r_{CH} is the distance between the nuclei C and H, and θ_x, θ_y, and θ_z are the angles that the C−H vector makes with the coordinate axes. For each of the phenyl rings, we have chosen the z-axis to be the para-axis of the ring, the x-axis is in the plane of the ring, and the y-axis is perpendicular to the plane. In the case of the *ortho*- and the *meta*-carbons, the experimentally measured dipolar frequency f_D actually has two components, namely, a coupling of the carbon to the ipso proton D_{C-Hi} and also to the proton at the ortho position D_{C-Ho}. The measured frequency is then obtained as[41] $[(D_{C-Hi})^2 + (D_{C-Ho})^2]^{1/2}$. The quaternary carbons have dipolar couplings to two equivalent protons in the ortho position. The meta protons being far away, their coupling may be neglected. In this case, the oscillation frequency may be obtained as $\sqrt{2}*(D_{C-Ho})$. The experimentally determined four oscillation frequencies for each phenyl ring are used to obtain the two order parameters S'_{zz} and $S'_{xx} - S'_{yy}$. In view of the uncertainty in the position of the H atom as determined by X-rays, it has been found necessary to vary the two C−C−H bond angles, which are found to deviate from the value of 120° corresponding to an ideal hexagonal geometry.[43,44] Accordingly, in the fitting procedure, the two C−C−H bond angles have also been slightly varied around 120°. Table 4 lists the oscillation frequencies and the local order parameters for each phenyl ring obtained in the smectic C phase at 120 °C by fitting the experimental data. Figure 8A and B shows the variation of S'_{zz} and $S'_{xx} - S'_{yy}$ as a function of temperature for all three rings. It is clear from Figure 8 and Table 4 that the order parameters differ by a small value between the three rings. It is also observed that the order parameters increase while passing from the nematic to the smectic C phase. Similar observation was made earlier in other systems exhibiting a smectic C phase at high magnetic fields.[45] The chemical shift values shown in Table 3 also further confirm this trend; the aromatic carbon chemical shifts are the largest at 120 °C and decrease monotonically at higher temperatures. The order parameters while entering the smectic phase from the nematic phase do not show a drastic change, which indicates that the conformer dynamics is nearly the same in both phases.

In order to estimate the orientation of the long axis of the molecular core with respect to the para-axes of the phenyl rings, one may use an uniaxial approximation and use the relations $S'_{zz}(1)/S'_{zz}(2) \approx P_2(\cos\beta_1)/P_2(\cos\beta_2)$ or $S'_{zz}(3)/S'_{zz}(2) \approx P_2(\cos\beta_3)/P_2(\cos\beta_2)$. However, a whole range of values of β_1, β_2, and β_3 will satisfy the above relation, and it is not possible to uniquely fix the orientaation of long molecular axis. To circumvent this problem, a relationship between the β's can be obtained using a method proposed earlier,[42,46,47] namely, $S'_{zz}(1)/S'_{zz}(2) \approx P_2(\cos\theta_{1-2})$ and $S'_{zz}(3)/S'_{zz}(2) \approx P_2(\cos\theta_{2-3})$, where θ_{1-2} and θ_{2-3} are the angles between the para-axes of rings 1 and 2 and 2 and 3, respectively. This is an approximation and is valid when one of the para-axes can be expected to be nearly parallel to the long molecular axis from physical considerations. From the information on the values of S'_{zz} of the three rings shown as a function of temperature in Figure 8, we have obtained average angles of 9.5 and 12.9° between the para-axes of rings 1 and 2 and

Table 4. Local Order Parameters of the Phenyl Rings and the Corresponding $^{13}C-^{1}H$ Dipolar Oscillation Frequencies for HyHPMAPD at 120°C[a]

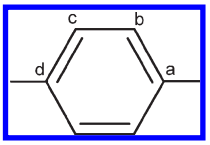

					calculated dipolar oscillation frequencies (kHz)			
120 °C	θ_b	θ_c	S'_{zz}	$S'_{xx} - S'_{yy}$	*b*	*c*	*a*	*d*
ring 1	120.3	120.9	0.75	−0.097	3.23	3.03	1.78	1.79
ring 2	120.1	120.8	0.79	−0.099	3.46	3.21	1.86	1.88
ring 3	120.1	120.3	0.74	−0.099	3.29	3.22	2.33[b]	1.76

[a] In the figure above the table, b and c are methine carbons, and a and d are quaternary carbons. [b] For carbon a in ring 3, the contribution of the azomethine proton has also been taken into account.

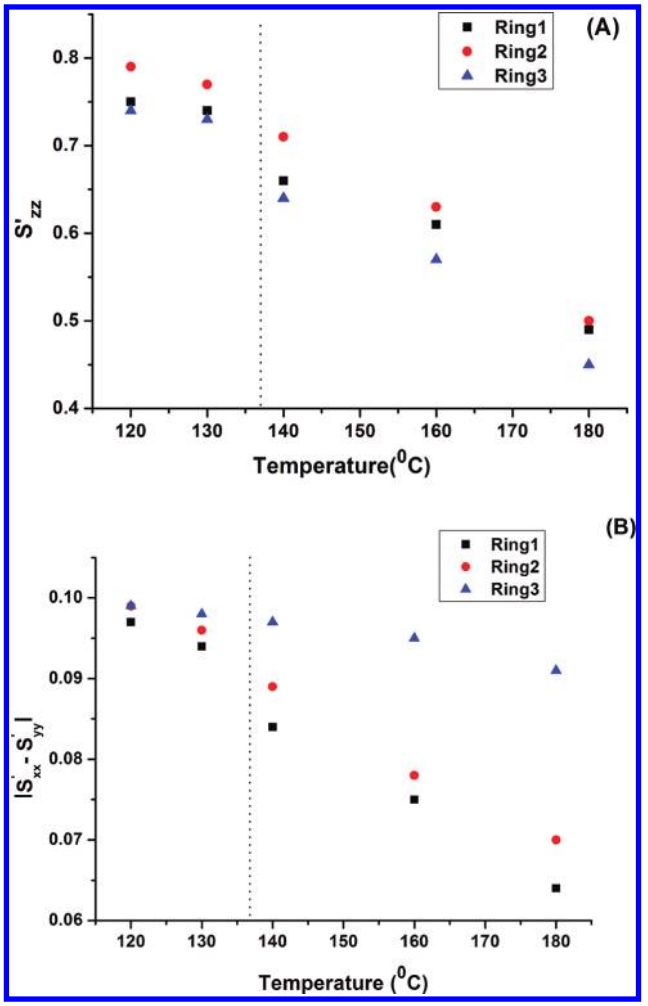

Figure 8. The variation of the order parameters S'_{zz} and $S'_{xx} - S'_{yy}$ as a function of temperature for HyHPMAPD in the mesophase.

rings 2 and 3, respectively. From the above information, an angle of 1° between the long axis of the molecular core and the para-axis of ring 2 was obtained. The order parameter values are typical for calamitic mesogens exhibiting the smectic C phase and nematic phase.[14,42] The negative values for $S'_{xx} - S'_{yy}$ are not unusual, being dependent on the choice of coordinates, and have been reported in other systems.[46] The estimation of the dipolar coupling of the carbon in the azomethine linking unit will require a knowledge of the complete order matrix, in the absence of any symmetry. In view of the lack of this information, one may use a uniaxial approximation and use only the dominant order parameter. Assuming the other order parameters to be small and negligible[48] and from the relation $D_{C-H} = K\{1/2(3\cos^2\theta - 1)S'_{zz}$ the angle θ between the long molecular axis and the azomethine CH bond vector may be calculated. Utilizing the order parameter of the long molecular axis that is found to coincide with the para-axis of the central phenyl ring and from the dipolar coupling of the azomethine carbons at different temperatures, an angle of 110.7 ± 0.4° has been obtained for the orientation of the CH bond of the azomethine carbon, which matches well with the value of 110.5° estimated in an earlier study on MBBA carried out using deuterium−carbon dipolar couplings.[49]

It may be mentioned that the ^{13}C chemical shifts provide one of the important means of determining the order parameters of the system.[42,46] This requires a knowledge of the CSAs of the carbon, which may be obtained either by experiments or by DFT calculations. In the present case, we have the information about CSA available from literature and from experiments for a few of the carbons of ring 1, and for these carbons, we have used the local order parameters obtained from the dipolar couplings to estimate the chemical shifts, and the results are presented in the Supporting Information. It is observed that the calculated values match reasonably well the experimental values and are also able to reproduce the trend in the variation of the chemical shifts as a function of temperature in both phases.

CONCLUSIONS

Novel three-ring-based mesogens built with three phenyl ring cores linked by ester and azomethine groups and hydroxy hexyloxy/alkoxy chains were synthesized by a multistep route. The HOPM and DSC data indicated enantiotropic nematic phase for all lower homologues and smectic C for higher homologues. Introduction of terminal hydroxyl has not altered the phase sequence, though it influenced the phase and thermal stability values. The ^{13}C NMR study of a representative hydroxyl-containing mesogen (HyHPMAPD) showed the parallel alignment of mesogens with the magnetic field in the smectic C and

nematic phases. The 2D SAMPI4 experiment provided $^{13}C-^{1}H$ dipolar couplings that were used to confirm the molecular structure of the mesogens and to compute the order parameters and the orientation of the molecular director. A large value for the local order parameters for all three rings in the smectic C phase of the mesogens has been obtained, which indicates that the lateral interactions of the core are dominant, a common feature of calamitic smectogens. In the nematic phase, the order parameter values are found to be in a range commonly observed in many nematic liquid-crystalline systems.

■ ASSOCIATED CONTENT

Supporting Information. The experimental details pertaining to the synthesis of mesogens as well as details regarding DSC data and plots of chemical shifts. This material is available free of charge via the Internet at http://pubs.acs.org.

■ ACKNOWLEDGMENT

T.N. would like to thank Dr. A. B. Mandal, Director, CLRI, for his support and encouragement. The partial financial support from NWP-23 is duly acknowledged. The use of the AV-III-500 Solid State NMR spectrometer funded by the Department of Science and Technology, New Delhi, at the NMR Research Centre, Indian Institute of Science, Bangalore, is gratefully acknowledged.

■ REFERENCES

(1) Kato, T.; Mizoshita, N.; Kishimoto, K. *Angew. Chem., Int. Ed* **2006**, *45*, 38.

(2) Tschierske, C. *Chem. Soc. Rev.* **2007**, *36*, 1930.

(3) Goodby, J. W.; Saez, I. M.; Cowling, S. J.; Gortz, V.; Draper, M.; Hall, A. W.; Sia, S.; Cosquer, G.; Lee, S.-E.; Raynes, P. *Angew. Chem., Int. Ed.* **2008**, *47*, 2754.

(4) *Handbook of Liquid Crystals*; Demus, D., Goodby, J. W., Gray, G. W., Spiess, H.-W., Vill, V., Eds.; Wiley-VCH: Weinheim, Germany, 1998.

(5) Hsu, H.-F.; Chen, H.-C.; Kuo, C.-H.; Wanga, B.-C.; Chiub, H.-T. *J. Mater. Chem.* **2005**, *15*, 4854.

(6) (a) Gray, G. W. *Molecular Structure and Properties of Liquid Crystals*; Academic Press: New York, 1962. (b) Luckhurst, G. R.; Gray, G. W. *The Molecular Physics of Liquid Crystals*; Academic Press: New York, 1979.

(7) (a) Tschierske, C. *J. Mater. Chem.* **1998**, *8*, 1485. (b) Tschierske, C. *J. Mater. Chem.* **2001**, *11*, 2647.

(8) (a) Yamaguchi, A.; Nishiyama, I.; Yamamoto, J.; Yokoyama, H.; Yoshizawa, A. *J. Mater. Chem.* **2005**, *15*, 280. (b) Weissflog, W.; Shreenivasa Murthy, H. N.; Diele, S.; Pelzl, G. *Philos. Trans. R. Soc. London, Ser. A* **2006**, *364*, 2657. (c) Donnio, B.; Buathong, S.; Bury, I.; Guillon, D. *Chem. Soc. Rev.* **2007**, *36*, 1495.

(9) Saez, I. M.; Goodby, J. W. *J. Mater. Chem.* **2005**, *15*, 26.

(10) (a) Goodby, J. W.; Gortz, V.; Cowling, S. J.; Mackenzie, G.; Martin, B. P.; Plusquellec, C. D.; Benvegnu, D. T.; Boullanger, D. P.; Lafont, E. D.; Queneau, E. Y.; Chamberte, E. S.; Fitremann, J. *Chem. Soc. Rev.* **2007**, *36*, 1971. (b) Vill, V.; Hashim, R. *Curr. Opin. Colloid Interface Sci.* **2000**, *7*, 395. (c) Jeffrey, G. A. *Carbohydr. Polym .* **1998**, *34*, 422.

(11) (a) Seed, A. J.; Toyne, K.; Goodby, J. W.; Hird, M. *J. Mater. Chem.* **1995**, *5*, 1. (b) Beekmans, F.; Boer, P. D. *Macromolecules* **1996**, *29*, 8726. (c) Chrzumnicka, E.; Szybowicz, M.; Bauman, D. *Z. Naturforsch., A: Phys. Sci.* **2004**, *59*, 510. (d) Van Boxtel, M. C. W.; Wubbenhorst, M.; Vanturnhout, J.; Bastiaansen, C. W. M.; Broer, D. J. *Liq. Cryst.* **2003**, *30*, 235. (e) Vij, J. K.; Kocot, A.; Perova, T. S. *Mol. Cryst. Liq. Cryst.* **2003**, *397*, 231/[531].

(12) (a) Dong, R. Y. *Nuclear Magnetic Resonance of Liquid Crystals*; Springer: New York, 1994. (b) Ramamoorthy, A., Ed. *Thermotropic Liquid Crystals: Recent Advances*; Springer: Dordrecht, The Netherlands, 2007; p 38. (c) Domenici, V.; Geppi, M.; Veracini, C. A. *Prog. Nucl. Magn. Reson. Spectrosc.* **2007**, *50*, 1.

(13) (a) Dvinskikh, S. V.; Yamamoto, K.; Scanu, D.; Deschenaux, R.; Ramamoorthy, A. *J. Phys. Chem. B* **2008**, *112*, 12347. (b) Sinha, N.; Ramanathan, K. V.; Berdague, P.; Judeinstein, P.; Bayle, J. P. *Liq. Cryst.* **2002**, *29*, 449.

(14) (a) Domenici, V.; Veracini, C. A.; Novotna, V.; Dong, R. Y. *ChemPhysChem* **2008**, *9*, 556. (b) Dong, R. Y.; Geppi, M.; Marini, A.; Hamplova, V.; Veracini, C. A.; Zhang, J. *J. Phys. Chem. B* **2007**, *111*, 9787.

(15) (a) Ciampi, E.; Furby, M. I. C.; Brennan, L.; Emsley, J. W.; Lesage, A.; Emsley, L. *Liq. Cryst.* **1999**, *26*, 109. (b) Auger, C.; Lesage, A.; Caldarelli, S.; Hodgkinson, P.; Emsley, L. *J. Phys. Chem. B* **1998**, *102*, 3718.

(16) (a) Zhang, J.; Domenici, V.; Veracini, C. A.; Dong, R. Y. *J. Phys. Chem. B* **2006**, *110*, 15193. (b) Dong, R. Y.; Chen, Y. B.; Veracini, C. A. *Chem. Phys. Lett.* **2005**, *405*, 177.

(17) Cardoso, M.; Figueirinhas, J. L.; Cruz1, C.; Van-Quynh1, A.; Ribeiro1, A. C.; Feio, G.; Apreutesei, D.; Mehl, G. H. *Mol. Cryst. Liq. Cryst.* **2008**, *495*, 348.

(18) (a) Fung, B. M. *Encycl. Nucl. Magon. Reson.* **1996**, *4*, 2744.(b) Ramanathan, K. V.; Sinha, N. In *Current Developments in Solid State NMR Spectroscopy*; Mueller, N., Madhu, P. K., Eds.; Springer-Verlag: Wienheim, Germany, 2003; Vol VIII.

(19) (a) Narasimhaswamy, T.; Lee, D. K.; Yamamoto, K.; Somanathan, N.; Ramamoorthy, A. *J. Am. Chem. Soc.* **2005**, *127*, 6958. (b) Zimmermann, H.; Bader, V.; Poupko, R.; Wachtel, E. J.; Luz, Z. *J. Am. Chem. Soc.* **2002**, *124*, 15286.

(20) (a) Courtieu, J.; Bayle, J. P.; Fung, B. M. *Prog. Nucl. Magn. Reson. Spectrosc.* **1994**, *26*, 141. (b) Caldarelli, S.; Hong, M.; Emsley, L.; Pines, A. *J. Phys. Chem.* **1996**, *100*, 18696.

(21) (a) Pratima, R.; Ramanathan, K. V. *J. Magn. Reson.* **1996**, *A118*, 7. (b) Dvinskikh, S. V.; Zimmermann, H.; Maliniak, A.; Sandstrom, D. *J. Magn. Reson.* **2003**, *163*, 46. (c) Narasimhaswamy, T.; Lee, D. K.; Somanathan, N.; Ramamoorthy, A. *Chem. Mater.* **2005**, *17*, 4567.

(22) Sudhakar, S.; Narasimhaswamy, T.; Srinivasan, K. S. V. *Liq. Cryst.* **2000**, *27*, 1525.

(23) Narasimhaswamy, T.; Srinivasan, K. S. V. *Liq. Cryst.* **2004**, *31*, 1457.

(24) Schroeder, D. C.; Schroeder, J. P. *J. Am. Chem. Soc.* **1974**, *96*, 4347.

(25) Schroeder, D. C.; Schroeder, J. P. *J. Org. Chem.* **1976**, *41*, 2566.

(26) Li, X.; Ying Zhang, W.; Zhu, L.; Zhang, B.; Zhang, H. *J. Mater. Chem.* **2009**, *19*, 236.

(27) Dixon, W. T. *J. Chem. Phys.* **1982**, *77*, 1800.

(28) Fung, B. M.; Khitrin, A. K.; Ermolaev, K. *J. Magn. Reson.* **2000**, *142*, 97.

(29) Nevzorov, A. A.; Opella, S. J. *J. Magn. Reson.* **2007**, *185*, 59.

(30) Wu, C. H.; Ramamoorthy, A.; Opella, S. J. *J. Magn. Reson.* **1994**, *A109*, 270.

(31) (a) Takegoshi, K.; McDowell, C. A. *Chem. Phys. Lett.* **1985**, *116*, 100. (b) Rhim, W. K.; Pines, A.; Waugh, J. S. *Phys. Rev. B* **1971**, *3*, 684.

(32) Sinha, N; Ramanathan, K. V. *Chem. Phys. Lett.* **2000**, *332*, 125.

(33) Levitt, M. H.; Suter, D.; Ernst, R.R. *J. Chem. Phys.* **1986**, *84*, 4243.

(34) Zhang, S.; Meier, B.H.; Ernst, R. R. *Phys. Rev. Lett.* **1992**, *69*, 2149.

(35) Ghosh, S; Mandal, P.; Paul, S.; Ranjt, P.; Neubert, M. E. *Mol. Cryst. Liq. Cryst.* **2001**, *365*, 703.

(36) Narasimhaswamy, T.; Monette, M.; Lee, D. K.; Ramamoorthy, A. *J. Phys. Chem. B.* **2005**, *109*, 19696.

(37) (a) Nakai, T.; Fujimori, H.; Kuwahara, D.; Miyajima, S. *J. Phys. Chem. B* **1999**, *103*, 417. (b) Das, B.; Grande, S.; Weissflog, W.; Eremin, A.; Schroder, M. W.; Pelzl, G.; Diele, S.; Kresse, H. *Liq. Cryst.* **2003**, *30*, 529.

(38) Fung, B. M. *Prog. Nucl. Magn. Reson. Spectrosc.* **2002**, *41*, 171.
(39) Das Bibhuti, B; Ajitkumar, T. G.; Ramanathan, K. V. *Solid State NMR* **2008**, *33*, 57.
(40) Jones, D. H.; Opella, S. J. *J. Magn. Reson.* **2006**, *179*, 105.
(41) (a) Nagaraja, C. S.; Ramanathan, K. V. *Liq. Cryst.* **1999**, *26*, 17. (b) Gan, Z. *J. Magn. Reson.* **2000**, *143*, 136.
(42) Dong, R. Y.; Xu, J.; Zhang, J.; Veracini, C. A. *Phys. Rev. E* **2005**, *72*, 061701.
(43) Fung, B. M.; Afzal, J.; Foss, T. L.; Chau, M.-H. *J. Chem. Phys.* **1986**, *85*, 4808.
(44) Xu, J.; Fodor-Csorba, K.; Dong, R. Y. *J. Phys. Chem. A* **2005**, *109*, 1998.
(45) (a) Marini, A; Domenici, V. *J. Phys. Chem. B* **2010**, *114*, 10391. (b) Poon, C. D.; Fung, B. M. *Liq. Cryst.* **1989**, *5*, 1159.
(46) Zhang, J.; Domenici, V.; Dong, R. Y. *Chem. Phys. Lett.* **2007**, *441*, 237.
(47) Catalano, D.; Cavazza, M.; Chiezzi, L.; Geppi, M.; Veracini, C. A. *Liq. Cryst.* **2000**, *27*, 621.
(48) Calucci, L.; Fodor-Csorba, K.; Forte, F.; Geppi, M. *J. Phys. Chem. B* **2011**, *115*, 440.
(49) Hohener, A.; Muller, L.; Ernst, R. R. *Mol. Phys.* **1979**, *38*, 909.